Temperature Dependence of Surface Crystallization in Bimorphic PET Fibers

C. J. DURNING, M. G. SCOTT, and H.-D. WEIGMANN, *Textile Research Institute and Department of Chemical Engineering, Princeton University, Princeton, New Jersey, 08540*

Synopsis

Open-bath, organic liquid treatments may be used to produce high surface area PET fibers through the action of liquid solvent-induced crystallization (SINC). It has been found that as the treatment bath temperature is increased, surface modification suddenly disappears. For a particular treatment method this occurs at a reproducible temperature, well below the liquid boiling point. A qualitative understanding of the mechanism of surface cavitation during liquid SINC is developed based on current descriptions of the component processes involved. These processes are: the glass–rubber transition, diffusion through rubbery and glassy polymer, and polymer–diluent crystallization. Although calculations of the threshold concentration for swelling support this conceptual framework, the absence of surface cavitation at higher treatment bath temperatures is not explained by it and is therefore attributed to an intervening phenomenon. Analysis of penetration depth data together with surface microscopy suggest the formation of a smooth surface layer interfering with normally observed cavitation at elevated temperatures. Manipulation of the extent of vapor precontact shows that vapor SINC prior to liquid exposure is most likely responsible for the smooth layer.

INTRODUCTION

The Textile Research Institute is conducting an ongoing investigation of the nature and applications of solvent crystallized poly(ethylene terephthalate) (PET) substrates. Previous workers have investigated the basic phenomenology with PET films.[1–5,18] Their work included elucidation of weight gain kinetics, supermolecular organization, effects of substrate orientation, as well as a tentative mathematical analysis. Additional work, germane to applications of such substrates, has produced bimorphic PET fibers[6] having a surface with a highly cavitated spherulitic morphology associated with solvent crystallized material and a core with a fibrillar structural typical of stress crystallized material. These fibers have both the mechanical integrity associated with conventional drawn PET fibers and a cavitated surface layer with an extremely high surface area. Such materials are of considerable interest, as they promise interesting applications in various polymer composite and textile systems.

Qualitatively, solvent-induced-crystallization (SINC) may be thought of in terms of constitutive processes: the glass–gel or glass–rubber transition, the diffusion of the solvent through both glassy and rubbery portions of the substrate, and polymer–diluent crystallization. Frisch[7] has categorized transport in noncrystallizable polymers according to the effect of the permeant on the glass transition temperature. When the dry glass transition temperature of the polymer is not far above the experimental temperature, an interactive permeant present in sufficient concentration may lower T_g below the environmental temperature. This situation corresponds to anomalous or Case II diffusion.

Journal of Applied Polymer Science, Vol. 27, 3597–3620 (1982)
 CCC 0021-8995/82/093597-24$03.40

Here, diffusion in glassy and rubbery regions coupled with glass–rubber transition kinetics leads to moving boundary phenomena and characteristically non-Fickian weight gain data. This has been observed for a variety of non-crystallizable systems.[8,9] A detailed mathematical description of this type of transport using a phase transformation approach has been worked out comparatively recently.[10,11] This moving boundary model is capable of rationalizing most of the existing data. Anomalous diffusion is encountered with amorphous, glassy PET; the dry glass transition at approximately 67°C may be decreased to as low as −90°C in the presence of certain interactive liquids.[3] Since PET is crystallizable, polymer–diluent crystallization is superimposed on the anomalous diffusion. Crystallization occurs within the region of the substrate which has undergone the glass transition.

The operation of these processes in concert produces a spherulitic, crystalline arrangement with a distribution of voids. Typically, for substances crystallized in liquid phase solvents, surface material appears highly cavitated, but cavitation drops sharply to a negligible value with depth into the sample regardless of substrate geometry. Hence the term "surface modified" is often applied. An interesting aspect of this type of surface modification which has been uncovered in recent work is discussed in this paper. When bimorphic fibers are produced by open-bath, liquid solvent contact, the surface modification suddenly disappears as the temperature of the liquid bath is increased. This disappearance is quite complete, and occurs at a temperature well below the solvent boiling point which is reproducible for a particular solvent and treatment method.

EXPERIMENTAL

Materials

Melt-spun, air-quenched PET filaments (360 denier), supplied by Allied Fibers and Plastics Co., were used as substrates. These filaments were characterized by density measurements and X-ray diffraction as completely amorphous. Since slow structural development can be induced in amorphous PET at room temperature, the samples were stored at low temperature until ready for use, at which time they were placed under standard conditions of 65% RH and 70°F for several hours.

Reagent grade methylene chloride ($MeCl_2$) and dimethyl formamide (DMF) obtained from J. T. Baker Chemical Co. were employed as received.

Treatment Techniques

PET substrates were exposed to various conditions of temperature and solvent contact by two different methods. A continuous treatment apparatus capable of exposing fiber to either liquid or vapor solvent at various temperatures and contact times was employed (Fig. 1). This apparatus is also capable of subsequently drawing the chemically modified fiber in a heating zone at various draw ratios. Primary residual solvent removal was accomplished by air drying in the case of methylene chloride and by a washing in a water bath in the case of DMF. The full description of this apparatus and its operation is given elsewhere.[6]

The second method of solvent exposure was to place the sample in a solvent

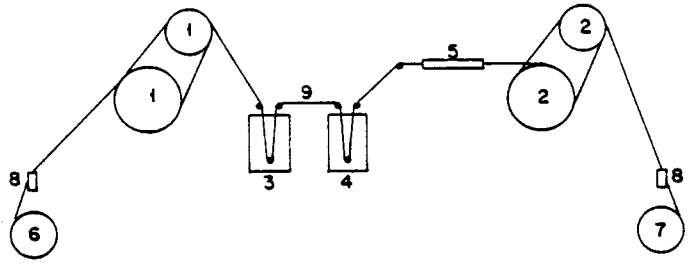

Fig. 1. Schematic representation of continuous treatment apparatus. (1) feed roll set; (2) takeup roll set; (3) solvent bath; (4) solvent exchange bath (used with DMF); (5) drawing zone; (6) filament supply; (7) skein winder; (8) tensioning devices; (9) threadline.

cell for a specified time interval. Separate cells for liquid and vapor exposure were constructed, and the temperature of the solvent was controlled. A mounting device was employed which enabled fibers to be held unrestrained or with any desired degree of extension. Only $MeCl_2$ was used in this immersion method, with primary residual solvent removal accomplished by air drying.

In all cases treated samples were dried under vacuum for 12 h. These samples were then frozen in sealed bottles until prepared for further analysis. Residual solvent remaining after this procedure was estimated for representative samples treated with $MeCl_2$; trace analysis for chlorine revealed levels of less than 1.5% $MeCl_2$ by weight remaining after vacuum drying.

Scanning Electron Microscopy

Owing to the complexity of transport involved, mathematical analysis of kinetic data is not presently possible for this system, and visual techniques were relied on to assess the effects of various solvent treatments. Scanning electron microscopy was employed extensively. Filament samples were mounted and coated with approximately 200 Å of gold–palladium to prevent discharging. These samples were observed, both longitudinally and in cross section, at magnifications of 200–2000×. Cross sections were produced by brittle fracture in liquid nitrogen. The microscopes employed were a type JSM by J.E.O. Co. and a model SMSM Super Mini by I.S.I. Inc.

Optical Microscopy

Cross sections of samples were also studied by optical microscopy. Treated fibers were mounted in epoxy resin capsules using the EPON 812 EPIKOTE kit obtained from E. M. Sciences, with a modified curing procedure, and microtomed to a thickness of ~10 μm. Microtomed sections were then mounted on glass slides and observed at 190–250× magnification using an E. Leitz Inc. Ortholux microscope.

Density Measurements

Sample densities were obtained using density gradient columns prepared according to ASTM standard D1505 with *n*-heptane and carbon tetrachloride. These solvents have been characterized as noninteractive with PET[12]; i.e., they

do not cause any substrate modification. Sample positions were read with a sensitive cathetometer after 72 h of settling time. Sample densities were then calculated by linear interpolation between standard float positions, with an estimated accuracy of ±0.2%.

RESULTS AND DISCUSSION

The effect of treatment bath temperature on surface texture is seen in Figures 2 and 3, which show longitudinal view scanning electron micrographs (SEM's) of PET fibers treated with $MeCl_2$ continuously with and without subsequent drawing to a draw ratio of 4. Liquid residence time was 7.6 s with treatment bath temperatures and draw ratios as indicated. With or without subsequent drawing, surface cavitation disappears at a bath temperature of about 20°C. The transition from a rough, cavitated surface to a smooth, unperturbed one is quite complete. Optical cross sections of undrawn samples are shown in Figure 4. Again the distinctly cavitated surface structure is clearly visible after treatment at the lower temperature, but not after treatment temperatures above 18–20°C.

Treatments with DMF give essentially the same results, although the disappearance of surface cavitation occurs at higher temperatures. Figure 5 shows longitudinal SEM's of samples treated continuously in DMF with liquid residences times of 3.6 s and a subsequent water wash of about 18 s. The filaments were drawn to a draw ratio of 4 with solvent treatment temperatures as indicated.

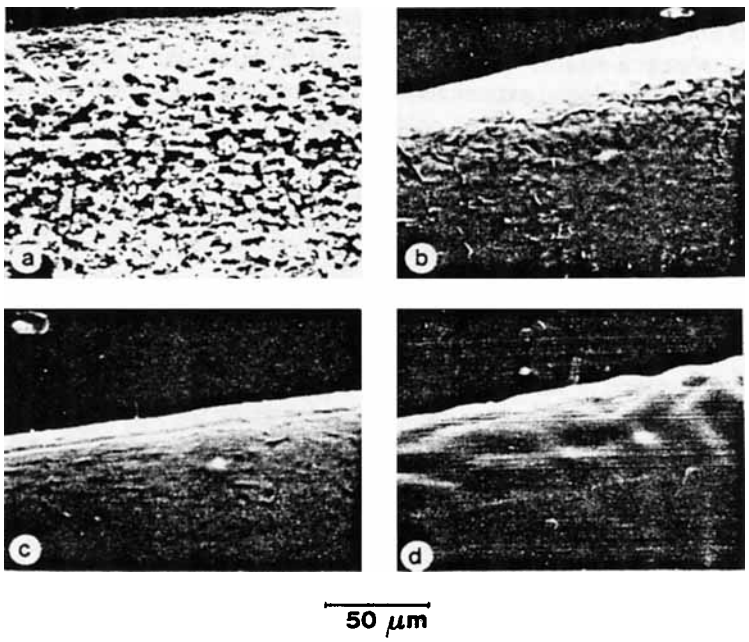

Fig. 2. Representative SEM's of the surface of PET filaments treated continuously with $MeCl_2$ solvent. Residence time in the liquid is 7.6 s with no subsequent drawing. Treatment bath temperatures: (a) 10°C; (b) 19°C; (c) 21°C; (d) 26°C.

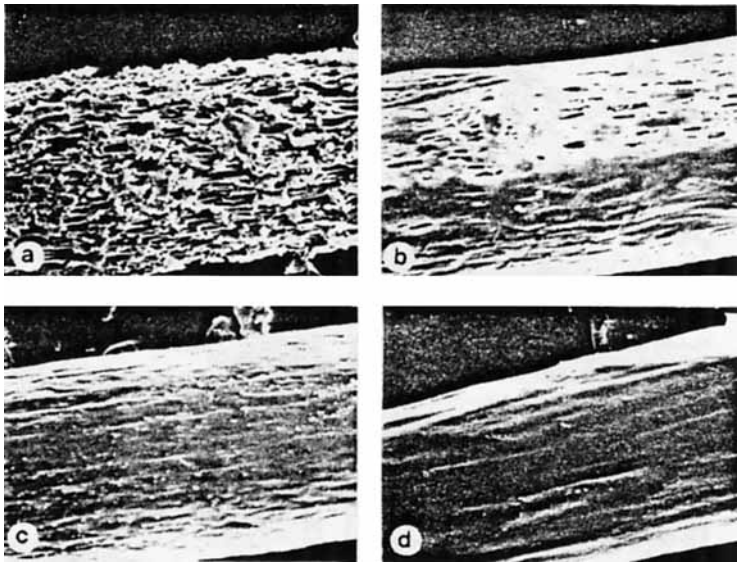

Fig. 3. Representative SEM's of the surface of PET filaments treated continuously with $MeCl_2$ solvent. Residence time in the liquid is 7.6 s with subsequent drawing to DR 4. Treatment bath temperatures: (a) 10°C; (b) 19°C; (c) 21°C; (d) 26°C.

Surface cavitation ceases above 40°C. Optical cross sections for drawn samples treated continuously in DMF are shown in Figure 6. Again surface cavitation is evident at lower temperatures and absent at higher temperatures, the transition occurring around 40°C.

The results obtained from the continuous treatments are repeatable and consistent. Similar effects were obtained when samples were exposed in the solvent immersion cell to chemical environments akin to those experienced in

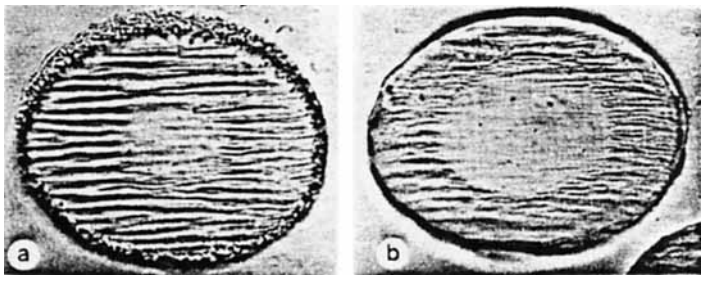

Fig. 4. Representative optical cross sections of PET filaments treated continuously with $MeCl_2$ solvent. Residence time in the liquid is 7.6 s with no subsequent drawing. Treatment bath temperatures: (a) 19°C; (b) 26°C. Note the distinct "penetration depth" demarking a region of the fiber which has undergone the glass–rubber transition.

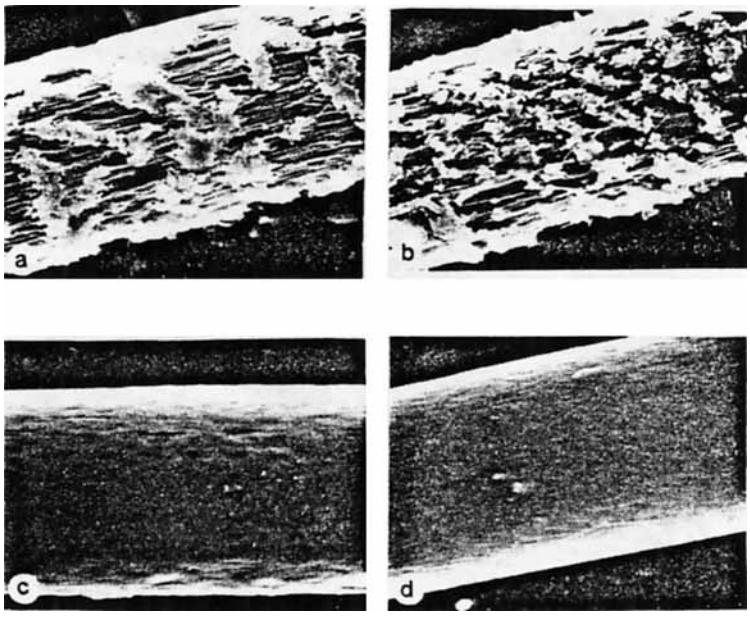

Fig. 5. Representative SEM's of the surfaces of PET filaments treated continuously with DMF solvent. Residence time in the liquid is 3.6 s with subsequent water wash and drawing to DR 4. Treatment temperatures: (a) 21°C; (b) 40°C; (c) 45°C; (d) 50°C.

the continuous treatment, i.e., an open solvent bath. However, in this treatment method any peculiarities associated with the continuous treatment are avoided, such as filament tension, roller contacts, or air and vapor flows. Methylene chloride was used as a model interactive agent for the immersion experiments. The high volatility of this liquid allows solvent removal by air drying, avoiding

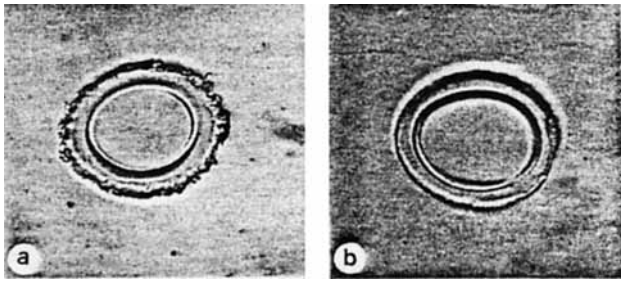

Fig. 6. Representative optical cross sections fo PET filaments treated continuously with DMF solvent. Residence time in the liquid is 3.6 s with subsequent water wash and drawing to DR 4. Treatment temperatures: (a) 40°C; (b) 50°C.

the need for a solvent exchange washing procedure. It should also be pointed out that, in the case of DMF, the treatments were conducted up to fairly high temperatures (80–100°C). Since this is at or above the dry glass transition temperature of the polymer, it is possible that thermally induced structural changes may interfere with permeant transport and SINC. The use of liquid $MeCl_2$ avoids this difficulty, because the observed change in surface texture occurs at much lower temperatures.

Figure 7 shows the results of 10-s immersions in liquid $MeCl_2$ at the indicated temperature levels with samples held unrestrained. The transition from cavitated to uncavitated surface structures occurs at approximately 30°C. Aside from the difference in the temperature at which surface cavitation disappears, the structures produced by immersion were identical to those observed after continuous treatments.

Although the mechanism responsible for the development of surface cavitation in amorphous crystallizable substrates crystallized by interactive liquids has not yet been satisfactorily determined, a qualitative understanding has been developed. Cavitation results from the rapid crystallization of a swollen, rubbery polymer, with accompanying exclusion of solvent from developing crystallites. The extent of cavitation should be directly related to the degree of swelling existing during crystallization. In exposing a PET substrate to a sudden change in external solvent activity, as when employing an open-bath solvent treatment, simultaneous solvent migration and solvent-induced crystallization occur. The

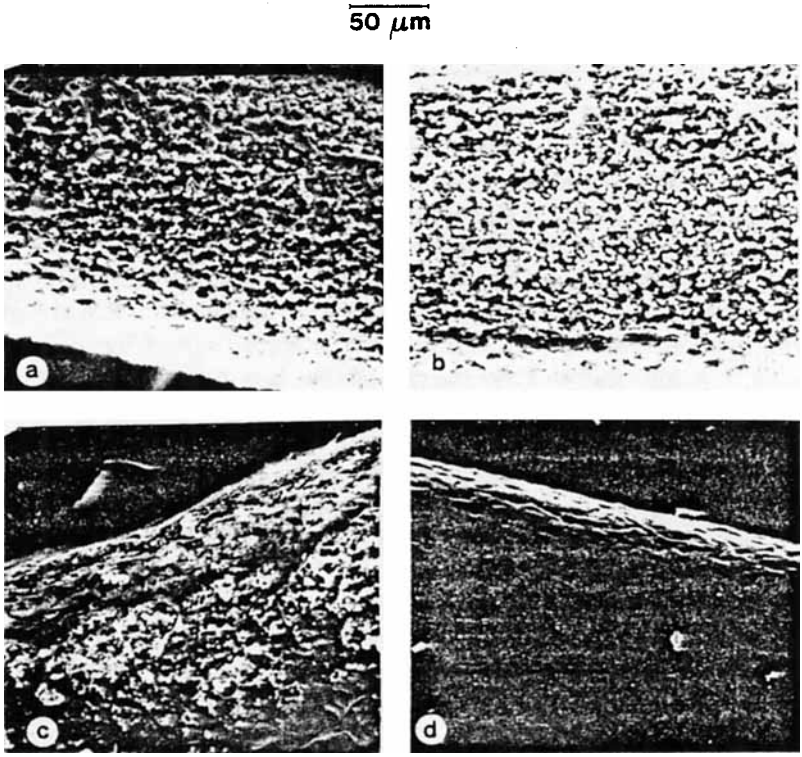

Fig. 7. Representative SEM's of the surfaces of PET filaments immersed unrestrained in $MeCl_2$ liquid for 10 s. Treatment temperatures: (a) 0°C; (b) 26°C; (c) 33°C; (d) 39°C.

local level of solvent concentration, and hence of swelling during crystallization, is determined by the coupling of transient permeation and local structural development.

The characteristics of this type of solvent transport have been examined by Makarewicz and Wilkes[2] for liquid phase 1,4-dioxane, methylene chloride, and acetone in PET films. After a short induction period, the moving boundary penetration depth, weight gain, and swelling kinetics for these systems display a $t^{1/2}$ dependence. The moving boundary is characterized by a morphological discontinuity which is reminiscent of solvent crazing discussed in connection with Case II transport systems.[13,14] It demarcates a region of the polymer which has undergone the glass–rubber transition and is capable of, or has already begun, crystallizing. This physical evidence suggests that the dynamics of transport in amorphous PET are somewhat analogous to those described mathematically by Astarita and Joshi[11] for transport in noncrystallizable, thick films.

In this description, the motion of the morphological discontinuity is determined by the microscopic processes involved in the glass–rubber transition which occurs at that discontinuity. For noncrystallizable systems, these processes have been characterized[13] as chain–chain slip, chain scission, and the onset of micro-Brownian motion. Sarti[14] has related the rate of these processes to the local level of solvent concentration above a threshold value at the discontinuity. The threshold value is that level of solvent concentration which provides sufficient free volume to allow large-scale chain mobility at the environmental temperature. Provided this threshold is relatively low, the kinetics of transport to achieve the threshold can be ignored. Hence the instantaneous rate of propagation of the front, and in turn the overall penetration depth kinetics, are largely governed by the level of solvent above threshold present at the front at any time.

This excess level of solvent at the morphological discontinuity is obviously the greatest when the accessibility of the front to the external solvent supply is greatest. Hence upon initial exposure the morphological front moves away from the sample surface with the highest velocity possible. As the penetration depth increases, the accessibility of the front to external solvent will diminish to the point where solvent diffusion to the front imposes a significant limitation. This situation has been observed experimentally for methanol in PMMA at 60°C.[15] Provided the sample is sufficiently large, a state limited by diffusion is approached asymptotically. Here the rate of the glass–rubber transition and hence the propagation of the morphological front occurs with a marginal excess of solvent above the swelling threshold value. This minimal driving force is provided by diffusion from the surface through the relatively large, already penetrated, rubbery portion of the sample. In this situation the penetration kinetics should be proportional to $t^{1/2}$. The dynamics involved are illustrated schematically in Figure 8(a).

This description of Case II transport can be adapted to provide an understanding of transport for crystallizable systems in which the effective glass transition temperature is lowered below the environmental temperature by the presence of the solvent. A quantitative estimate of the threshold concentration for the glass–rubber transition at 25°C in PET can be made by employing the Kelly–Bueche equation.[16] This relationship expresses the glass transition temperature of a polymer–diluent mixture in terms of the physical properties

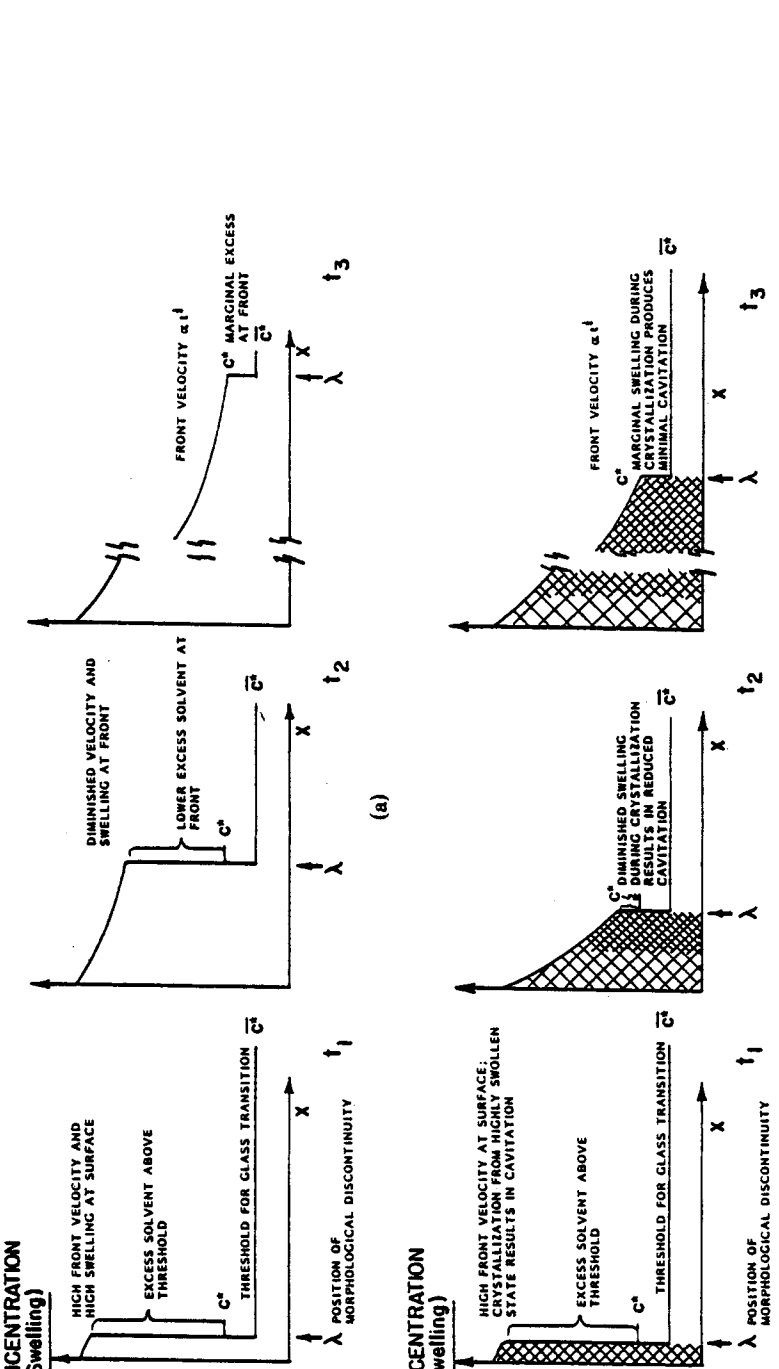

Fig. 8. Schematic comparisons of developing concentration profiles during case II diffusion with (b) and without (a) developing crystallinity. λ shows the position of morphological discontinuity. Cross hatching represents crystallinity; tighter hatching implies lower cavitation. Profiles are shown at three different times; from left to right: the initiation of transport, during non-Fickian induction period, and the diffusionally limited asymptote. Extremely rapid crystallization is assumed. C^* and $\bar{C}^*$ have the same meaning as in Ref. 11.

of the dry polymer and pure solvent, based on free volume theory. By assuming additivity of polymer and solvent volumes, rearrangement of the equation gives an expression for the threshold concentration:

$$\overline{C}^* = \rho_s \left[\frac{\alpha_s}{\Delta\alpha_p} \left(\frac{T - T^\circ_{g_s}}{T^\circ_{g_p} - T} \right) + 1 \right]^{-1} \tag{1}$$

where $\overline{C}^*$ is the threshold mass concentration at the environmental temperature T (the same nomenclature used by Astarita and Joshi[11]), ρ_s is the pure solvent density, α_s is the thermal expansion coefficient of the solvent, $\Delta\alpha_p$ is the change in the thermal expansion coefficient at the glass transition, and $T^\circ_{g_p}$ and $T^\circ_{g_s}$ are the glass transition temperatures of the dry polymer and pure solvent. The last quantity is seldom known experimentally, but other workers[17] have employed a value of 50 K below the solvent freezing point with satisfactory results.

For solvent crystallized polymers with a low overall void content and moderate levels of crystallinity, the ratio of the threshold mass concentration for swelling to the equilibrium mass concentration in amorphous areas can be calculated from

$$\frac{\overline{C}^*}{C^\circ} = \rho_s \left[\frac{\alpha_s}{\Delta\alpha_p} \left(\frac{T - T^\circ_{g_s}}{T^\circ_{g_p} - T} \right) + 1 \right]^{-1} \left\{ \frac{X^\infty [\Phi\rho_c/(1 - \Phi) + \rho_a]}{1 + X^\infty \rho_a/\rho_s} \right\}^{-1} \tag{2}$$

Here C° is the equilibrium solvent mass concentration in amorphous regions, X^∞ is the overall equilibrium solvent mass fraction, Φ is the overall polymer volume fraction crystallized at equilibrium, and ρ_c and ρ_a are the polymer crystalline and amorphous phase densities in the absence of solvent.

Table I shows threshold concentrations and concentration ratios for various PET and polycarbonate (PC)–solvent systems calculated from eqs. (1) and (2). (It should be noted that bisphenol A polycarbonate is similar to PET in that it can be quenched below its glass transition temperature without significant crystallization. Exposure to interactive liquids leads to crystallization and transport phenomena similar to those found for PET.[17]) The physical data employed for these calculations are contained in Table III. The ratio $\overline{C}^*/C^\circ$ is indicative of the ability of a liquid to induce the glass–rubber transition and hence induce crystallinity. The liquids are arranged in order of increasing value of this ratio, corresponding to decreasing capability of inducing crystallinity. This order

TABLE I
Values of Threshold Concentration and Ratio of Threshold to Equilibrium Concentration at 25°C

Liquid	$\overline{C}^*$(g/cm³)	$\overline{C}^*/C^\circ$	
PET			
$MeCl_2$	0.059	0.081	
DMF	0.053	0.100	Decreasing
Acetone	0.035	0.121	capability
Nitromethane	0.080	0.188	for inducing
H_2O[a]	0.095	7.21	crystallinity
PC			
Acetone	0.149	0.475	
CCl_4	0.452	0.561	
Methanol[a]	0.136	2.00	

[a] Does not induce crystallinity.

agrees well with other indices of interactiveness employed by previous authors[3,12] to characterize PET–diluent systems. Note the case of water, which is incapable of crystallizing PET at room temperature and hence has a ratio $\bar{C}^*/C^\circ$ greater than 1. For $MeCl_2$ and DMF in PET, the ratios $\bar{C}^*/C^\circ$ are fairly small. One might therefore justifiably neglect the kinetics of sorption to attain the threshold concentration when analyzing the overall sorption kinetics of these systems. For other liquids in PET and for the polycarbonate systems, this may be a poor approximation, because the ratio $\bar{C}^*/C^\circ$ has a significantly larger value.

Makarewicz and Wilkes[3] have demonstrated that crystallization in thick PET films under conditions of swelling occurs on a much shorter time scale than overall transport for many organic permeants including $MeCl_2$. This suggests that, in a dynamic situation, the complete crystallization of swelled material occurs just behind the moving morphological front. Except for very small geometries, the extent of crystallization of a sample should closely follow the extent of penetration. That this is true for the filaments studied in this work is shown in Figure 9. Here penetration depth kinetics assessed by SEM are compared with crystallization kinetics obtained from density measurements on a 360-den, as-spun polyester filaments exposed to liquid $MeCl_2$ at 40°C. This provides a qualitative understanding of the production of surface modification. Since crystallization occurs just behind the morphological discontinuity, it occurs at a level of swelling similar to that at the front. Hence, upon initial exposure to external solvent, crystallization occurs at high levels of swelling. In this surface layer the extremely rapid locally inhomogeneous densification and concomitant high volume of solvent exclusion results in a highly cavitated structure. Conversely, in the diffusionally limited situation, crystallization occurs at relatively low levels of swelling, and subsequent cavitation is much less severe. Additionally, since crystallites can be considered impenetrable by solvent, they tend to decrease the accessibility of the front to external solvent rapidly so that the approach to diffusional limitations occurs after relatively small penetration depths. This framework provides a convenient rationalization of the predominance of $t^{1/2}$ dependencies in the penetration and weight gain data on relatively

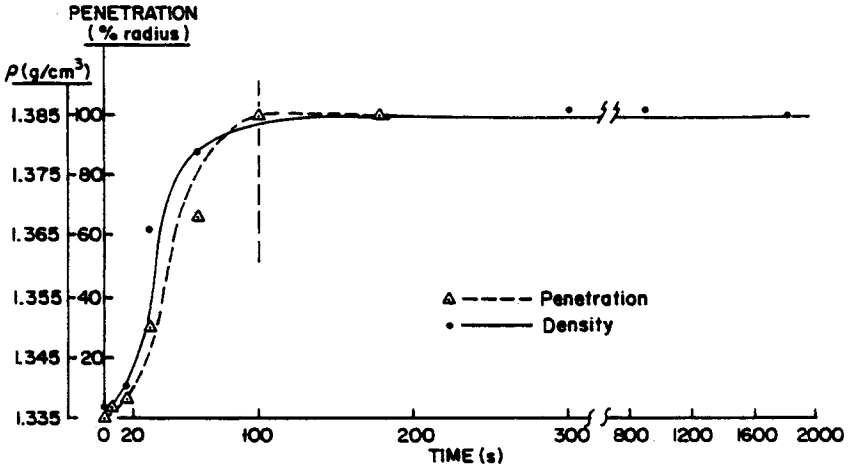

Fig. 9. Comparison of penetration depth assessed by SEM and overall degree of crystallinity assessed by density. The vertical dashed line indicates the point of complete penetration: (▲ ---) penetration; (● —) density.

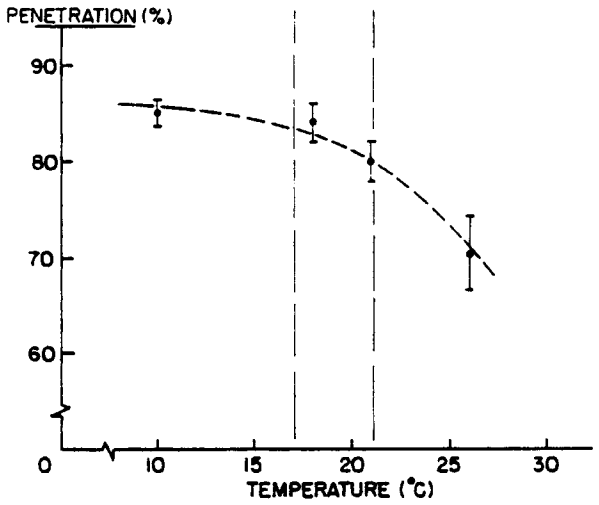

Fig. 10. Percent radial penetration assessed from cross sections of undrawn PET filaments exposed continuously to $MeCl_2$ liquid as a function of treatment bath temperature. Residence time in the liquid is 7.6 s. Vertical dashed lines indicate the region of transition from rough to smooth surface.

thick PET films observed by Makarewicz and Wilkes.[3] A schematic comparison of the transport in thick films involving crystallization with usually observed Case II transport is provided in Figures 8(a) and 8(b).

These qualitative considerations of SINC would appear to preclude the observed anomalous temperature dependence of fiber surface modification. The important temperature sensitive factors governing transport and morphological

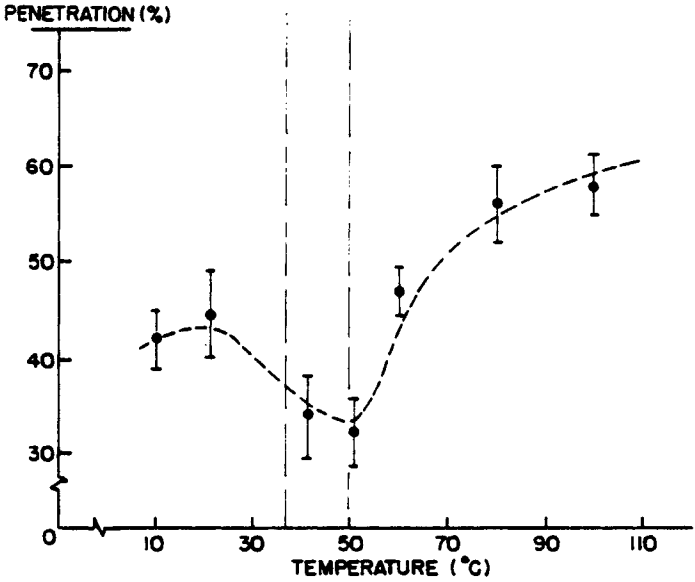

Fig. 11. Percent radial penetration assessed from cross sections of undrawn PET filaments exposed continuously to DMF liquid as a function of treatment bath temperature. Residence time in the liquid is 3.6 s. Vertical dashed lines indicate the region of transition from rough to smooth surface.

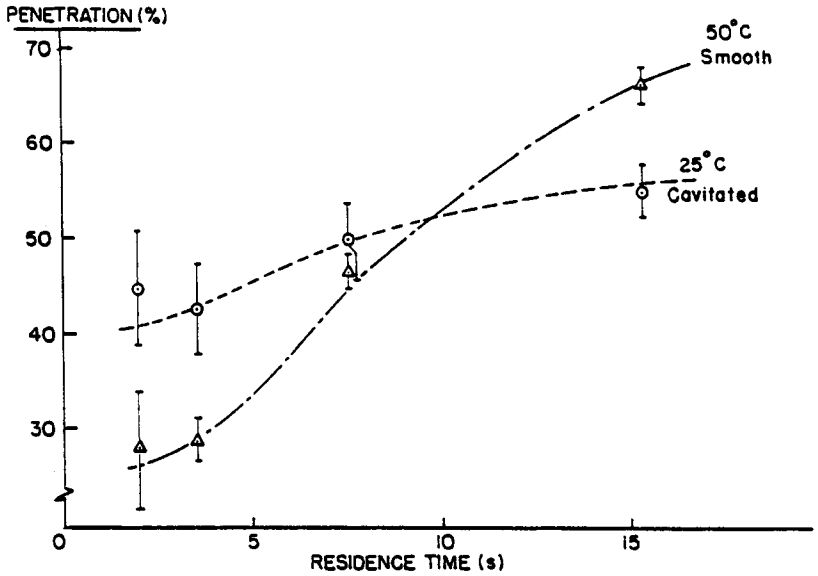

Fig. 12. Penetration depth kinetics for undrawn PET filaments exposed continuously to DMF liquid.

development are easily identified. They are the diffusivity in the rubbery crystallizing region, the glass–rubber transition kinetics at the morphological front, and the level of spherulitic morphology developed in the rubbery penetrated polymer. The temperature dependence of diffusivity above the glass transition in polymeric systems is adequately described by free volume theory.[19–21] At finite permeant concentrations, diffusivities should display a moderate, nearly temperature-independent activation energy. (In semicrystalline systems, the crystalline phase may be considered impermeable. Various chain restrictions occur in the presence of crystallites[22] which affect the magnitude of the amorphous diffusivity. For moderate crystallinity, as is encountered in PET crystallized by liquids, the free volume theory may be directly applied to amorphous regions to adequately describe temperature dependence.) Jameel et al.[5] have reported an activation energy of 9.7 kcal/mol for DMF diffusion above glass transition in slightly drawn PET films. Studies on noncrystallizable polymers show an Arrhenius temperature dependence of the glass–rubber transition kinetics with large values of activation energy (40–60 kcal/mol).[13,14] It is assumed that the glass–rubber transition in amorphous PET occurs by essentially the same mechanisms as in noncrystallizable systems. Finally, for polymer–diluent crystallization in PET, Makarewicz[1] has observed little temperature dependence of the level of crystallinity achieved in the presence of a particular permeant.

In view of the previous discussion concerning the dynamics of transport [see Figs. 8(a) and 8(b)], one expects that for short exposure times the temperature dependence of the glass–rubber transition will dominate the temperature dependence of the penetration depth. For long exposure times, i.e., in the diffusionally limited situation, the temperature dependence of the penetration depth is more complex and reflects both the temperature dependence of the glass–rubber transition and that of the diffusivity in the rubbery penetrated

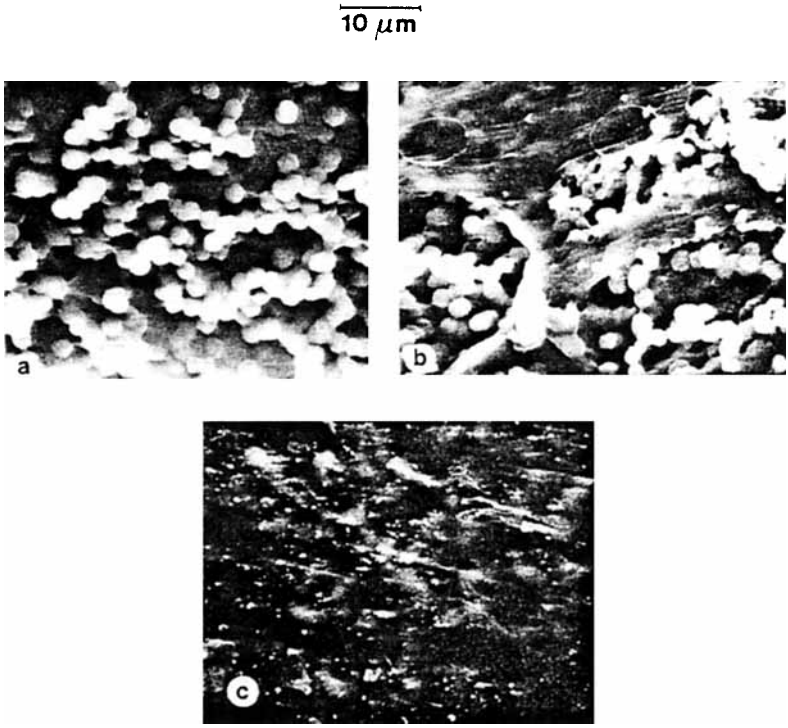

Fig. 13. Representative SEMs of the surfaces of PET filaments immersed unrestrained in $MeCl_2$ liquid for 10 s. Treatment temperatures: (a) 0°C; (b) 33°C; (c) 39°C. Note partial surface coating at 33°C.

region. In either case a positive temperature coefficient of penetration depth observed at a particular exposure time is expected. In other words, a monotonically increasing plot of penetration depth at a particular exposure time vs. temperature should result, though not necessarily reflecting the influence of a single process.

Contrary to this expectation, assessment of penetration depth at constant immersion times in open-bath treatments as a function of liquid bath temperature by examination of a statistical number of cross sections results in monotonically decreasing or nonmonotonic functionalities. Figures 10 and 11 show such data for undrawn filaments exposed continuously to $MeCl_2$ and DMF for 7.6 s and 3.6 s, respectively. Both plots display anomalous temperature effects in the neighborhood of the transition from rough to smooth surface textures. In the case of DMF the expected increasing temperature dependence is observed outside of the region where the transition in surface morphology occurs. For $MeCl_2$ this is not obvious because of the somewhat limited temperature span.

Examining the kinetics of the penetration depth for DMF above and below the transition region yields further detail concerning the nature of the change in surface structure with temperature. Figure 12 shows a splot of these kinetics assessed from a statistical number of cross sections at 25°C (rough, cavitated surface) and 50°C (smooth surface). Note an enhancement in overall penetration rate at the higher temperature. Contrary to prediction, the 50°C curve lies below the 25°C curve in the initial portion of the plot. This suggests an initial

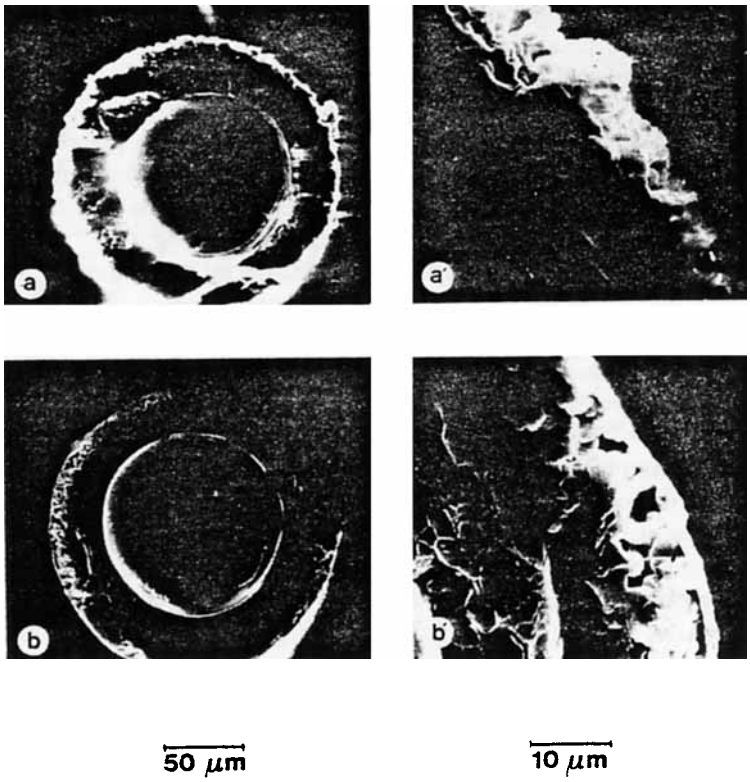

Fig. 14. Representative SEMs of the brittle fracture cross sections of PET filaments immersed unrestrained in $MeCl_2$ liquid for 2 s. Treatment temperatures: (a,a') 26°C; (b,b') 35.5°C. Note skinlike surface layer covering filament at higher treatment temperature.

retardation in penetration associated with the formation of a smooth surface. The transition to smooth surface texture seems to result from an intervening, local surface phenomenon which prevents normal initiation of liquid transport.

Direct observations of both rough and smooth surface filaments produced by immersions in $MeCl_2$ were made at high SEM magnifications to determine the detailed surface structures involved. Figure 13 shows longitudinal views of filaments immersed for 10 s, while Figure 14 shows brittle fracture cross sections of filaments immersed for 2 s. These micrographs indicate the presence of a thin layer of smooth polymeric material which partly obscures the normally cavitated surface at elevated temperatures. These completely smooth surfaces consist of a contiguous "coating" formed at the surface, with the expected liquid-modified, cavitated structure just beneath. This is particularly vivid in the high magnification fracture cross sections shown in Figure 14.

This evidence, together with the penetration kinetics previously discussed, leads to the conclusion that a smooth surface layer of polymeric material is produced just prior to or during initial liquid bath contact. The layer is apparently stable at elevated temperatures such that it can withstand swelling stresses and other destructive influences produced by subsequent liquid exposure, and the normally observed surfaces cavitation is eliminated. Three possible mechanisms for the formation of such a surface layer exist: oligomer and low

molecular weight polymer extraction followed by redeposition on the surface, high polymer surface layer gelation or dissolution followed by redeposition, and vapor phase SINC just prior to liquid contact. Each mechanism and its implications are considered briefly.

Oligomer and low molecular weight polymer extraction followed by redeposition on the surface has been studied for PET substrates immersed in interactive liquids.[23] This phenomenon does not show a strong temperature dependence. Redeposition occurs as discontinuous platelets and fibrils and cannot satisfactorily account for the formation of a contiguous coating.

High polymer surface layer gelation followed by rapid deswelling has been studied for nylon 6 fibers swelled in zinc chloride solutions.[24] Such treatments produce surface coatings of various textures. Recent patent literature[25] has proposed the possibility of producing textured surface coatings with melt-spun, crystallizable polymer fibers, including PET, by treatment with low-boiling-point organic liquids. The mechanism of this process is discussed in terms of surface layer dissolution followed by redeposition. Surface coatings produced by this procedure are textured but not completely dissimilar to those observed at elevated temperature in this work. Since the solvating power of a liquid is an increasing function of temperature, such a mechanism is at least feasible. Experimental observations, however, discount this possibility. If such a mechanism were operative, one would expect the temperature of transition in surface texture to depend strongly on liquid exposure time, since solvation is a time-dependent process. No shift in the temperature of surface texture transition is observed with changes in liquid exposure time in either the continuous treatments or the immersions.

A satisfactory, self-consistent mechanism felt to be responsible for the smooth surface layer produced at elevated temperatures is that of vapor phase SINC just prior to liquid bath exposure. Vapor phase SINC has not been investigated as extensively as liquid phase SINC. Makarewicz and Wilkes[2] have done some preliminary investigations with PET films. The vapor-modified surface is relatively smooth and uncavitated when compared with the liquid-treated surface. Small-angle light scattering has shown that vapor-modified substrates have a spherulitic, semicrystalline morphology comparable to the liquid-modified variety except for the pronounced surface cavitation of the latter. Table II shows density measurements on $MeCl_2$-treated filaments which indicate that the final levels of crystallinity attained by extended treatments in saturated vapor are nearly identical to the final levels achieved in liquid phase immersions. These data also show the kinetics of vapor phase SINC to be significantly slower than in the corresponding liquid phase situation.

Figure 15 shows longitudinal SEM's illustrating the effect of DMF vapor, with and without subsequent drawing, using the continuous treatment method. The residence time in saturated vapor is 20.3 s at 50°C, just above the temperature at which the transition in surface texture is initially observed with this apparatus. The surfaces appear smooth, with a noncavitated, apparently semicrystalline structure revealed at high magnifications. Cross sections of these samples (Fig. 16) show a thin, smooth outer coating such as that proposed to be interfering with surface modification in high temperature open-bath solvent treatments. The same morphologies are observed for samples exposed to saturated $MeCl_2$ vapor at 39°C in the immersion cell. Figure 17 shows longitudinal SEM's of these

TABLE II
Density and % Crystallinity for 360 Denier, As-Spun PET Monofilaments Exposed to Various $MeCl_2$ Environments

Exposure time (s)	Bath temp (°C)	Density (g/cm³)	Crystal. (%)
Liquid phase exposure			
10.0	23.5	1.383	40.0[a]
10.0	26.0	1.384	40.8[a]
10.0	29.2	1.383	40.0[a]
10.0	33.0	1.385	41.6[a]
10.0	39.8	1.386	42.5[a]
Vapor phase exposure			
5.0	39.8	1.337	1.6
15.0	39.8	1.340	4.2
180.0	39.8	1.3847	41.4[a]
300.0	39.8	1.3860	42.5[a]
900.0	39.8	1.3860	42.5[a]
1800.0	39.8	1.3847	41.4[a]

[a] Indicates complete penetration of sample.

samples at various treatment times, revealing smooth, uncavitated surfaces. Figure 18 shows brittle fracture cross sections for these fibers as viewed in the SEM, which show the penetration depth of the morphological front and the uncavitated nature of the vapor-modified surface for various contact times.

In an open-bath treatment the fiber briefly passes through a region of intimate

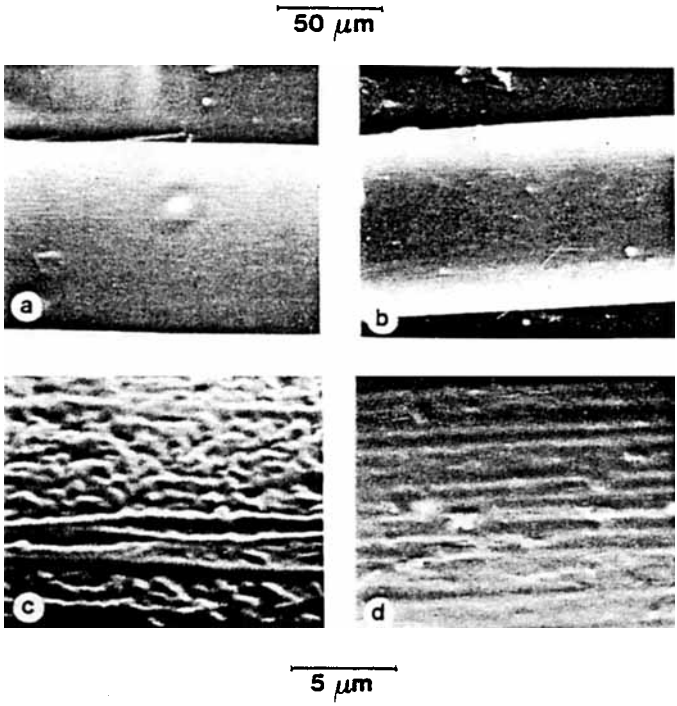

Fig. 15. Representative SEM's of the surfaces of PET filaments treated continuously with DMF vapor. Residence time in the saturated vapor is 20.3 s at a treatment temperature of 50°C. Draw ratios for subsequent drawing: (a,c) DR 1; (b,d) DR 4.

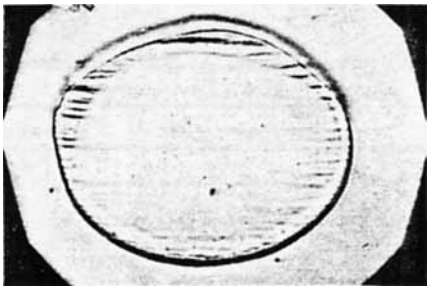

Fig. 16. Representative optical cross section of PET filament treated continuously with DMF vapor. Residence time in the saturated vapor is 20.3 s at a treatment temperature of 50°C with no subsequent drawing.

contact with the interactive vapor above the liquid surface. The extent of this vapor contact depends on the physical arrangement of the liquid treatment bath, i.e., the fiber residence time in the "vapor space" above the liquid surface. The severity of the vapor's effect on the fiber is directly related to its vapor pressure, which is a strong function of temperature as expressed by the well-known Antoine

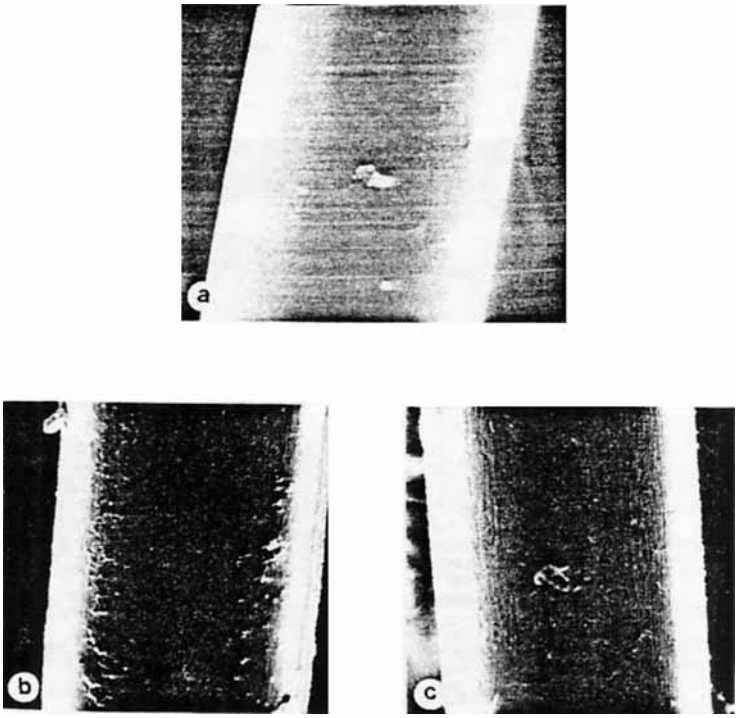

Fig. 17. Representative SEM's of the surfaces of PET filaments exposed to saturated $MeCl_2$ vapor at 39°C. Treatment durations: (a) 5 s; (b) 30 s; (c) 60 s. Note lack of surface cavitation.

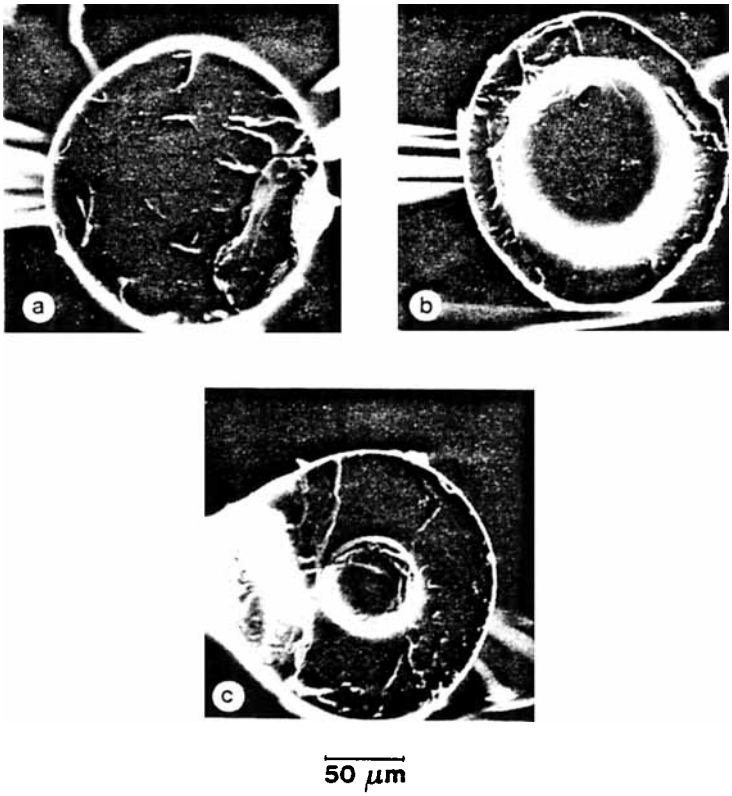

Fig. 18. Representative SEM's of brittle fracture cross sections of PET filaments exposed to saturated $MeCl_2$ vapor at 39°C. Treatment durations: (a) 5 s; (b) 30 s; (c) 60 s. Note the clearly visible depth of penetration demarking a region of the fiber which has undergone the glass–rubber transition.

equation. At first glance, then, a mechanism precluding surface cavitation based on vapor-induced surface modification provides a basis for understanding the difference in the temperature of transition in surface texture observed in the two different treatment methods, since different extents of vapor contact are realized. This mechanism also explains the temperature effects on surface morphology observed with both treatment techniques, which result from the vapor's increased capacity for producing uncavitated, semicrystalline surface layers at higher vapor pressures.

The mechanism implies that the changeover from cavitated to smooth surfaces with increasing temperature is in fact a gradual one which becomes apparent suddenly at a particular temperature. At low temperatures, the vapor pressure is low, and surface layers produced by limited vapor precontact are relatively insignificant. Subsequent liquid contact destroys their integrity by virtue of the extensive swelling and cavitation which takes place. Remnants of such coatings have been observed in SEM's quite clearly and regularly on a statistical number of samples. These fragments become more numerous as the temperature of transition in surface texture is approached. At higher temperatures the vapor-crystallized surface layer produced by limited precontact is significantly thicker and more stable, to the point where it can remain contiguous when sub-

TABLE III
Physical Data for Calculation of Threshold Concentrations and Ratios $\bar{C}^*/C^\circ$

Polymer Properties		
PET	$T_{gp}^0 = 343$ K	$\rho_p = 1.335$ g/cm^3
	$\alpha_s/\Delta\alpha_p = 5.71$[a]	$\rho_{cry} = 1.455$ g/cm^3
Polycarbonate	$T_{gp}^0 = 422$ K	$\rho_p = 1.2$ g/cm^3
	$\alpha_s/\Delta\alpha_p = 3.16$[a]	$\rho_{cry} = 1.35$ g/cm^3

Characteristics of liquid-induced crystallinity at 25°C

Liquid	ρ_s^b (g/cm^3)	Freezing point[b] (°C)	x^∞	ϕ
PET				
Methylene chloride	1.336	−96.7	0.42[c]	0.434[f]
Nitromethane	1.1312	−28.6	0.19[c]	0.492[f]
Acetone	0.792	−94.6	0.10[c]	0.583[f]
DMF	0.945	−58.3	0.565[d]	0.195[g]
H_2O	1.00	0.0	0.02[e]	0.0
Polycarbonate				
Acetone	0.79[h]	−94.6[h]	0.24[i]	0.30[i]
CCl_4	1.58[h]	−23.0[h]	0.69[h]	0.30[i]
Methanol	0.79[h]		0.062[h]	0.0

[a] Assumes a typical value for the solvent thermal expansion coefficient of 1.2×10^{-3} k^{-1}.
[b] Data from Lange's *Handbook of Chemistry*, 12th ed.
[c] Data from Ref. 3.
[d] Data from Ref. 5.
[e] Upper boundary value.
[f] Data from Ref. 18.
[g] Unpublished data.
[h] Data from Ref. 17.
[i] Upper boundary value.

sequently immersed in the liquid environment. This densified layer of surface material inhibits the characteristically rapid initial liquid phase penetration and swelling, as observed when analyzing penetration depth data. This process is also consistent with the observation that there is no effect of liquid immersion time on the temperature of transition from cavitated to smooth surfaces, since only the extent and severity of vapor precontact determine the integrity of surface layers which inhibit cavitation.

From this understanding of the underlying processes responsible for the observed anomalous temperature dependence of surface modification, one can draw certain conclusions. If the transition in surface texture is due to vapor precontact, surface cavitation should be inhibited or produced at will, regardless of the liquid bath temperature, by carefully controlling the extent of precontact. In particular, at low temperatures where surface cavitation is normally observed with both treatment methods, smooth surface fibers should result by deliberately exposing the filament to extended vapor contact prior to low temperature liquid contact. By similar reasoning, at high temperatures where the original treatments normally result in smooth surface fibers, cavitated fibers should result if the vapor space above the liquid surface is eliminated.

Direct experimental verification of these predictions has been achieved. Figure 19 shows longitudinal SEM's of as-spun PET fibers treated continuously

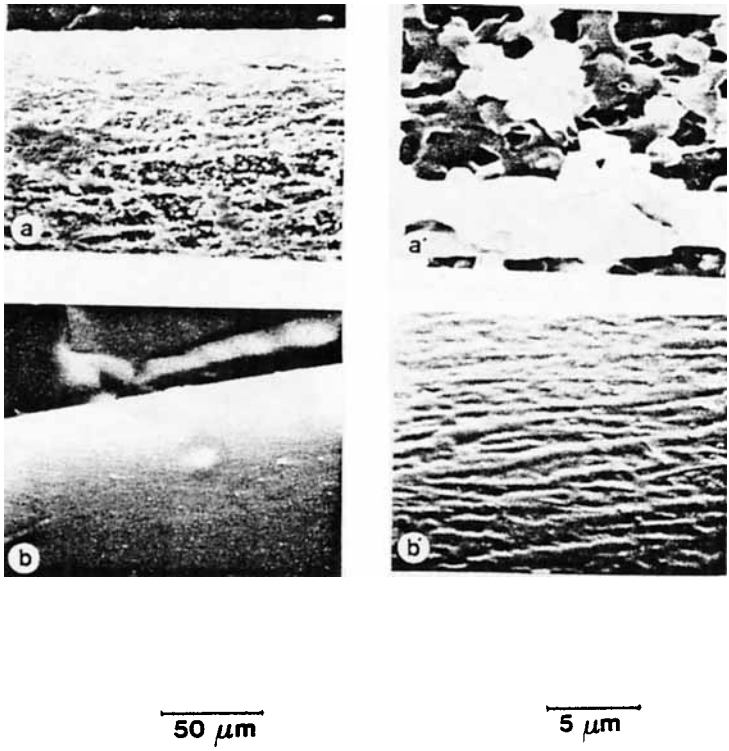

Fig. 19. Representative SEM's of the surfaces of undrawn PET filaments treated continuously in (a) 24°C DMF liquid only for 6.1 s; (b) 50°C DMF vapor for 20.3 s followed by 24°C DMF liquid for 6.1 s; (a') and (b') higher magnifications of (a) and (b). Note that the cavitated surface is obscured by deliberate vapor precontact.

with DMF vapor only at 50°C for 20.3 s, followed by 6.1 s in DMF liquid only at 24°C. Note the smooth surface produced compared with the liquid only treatment at 24°C; the deliberately extensive vapor precontact has produced a surface layer sufficiently stable to preclude the normally observed cavitation at this temperature. The cross section shown in Figure 20 reveals the smooth surface and also shows the morphological front caused by DMF migration during subsequent liquid phase contact.

Figure 21 shows longitudinal SEM's of filaments treated continuously with both vapor and liquid phase DMF at 50°C. As pointed out above, smooth fibers

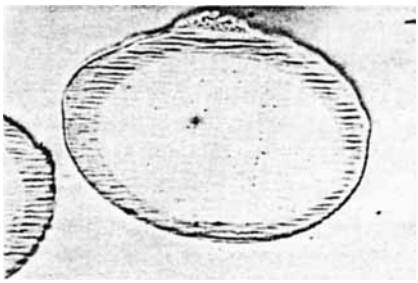

Fig. 20. Representative optical cross sections of undrawn PET filaments treated continuously with 50°C DMF vapor for 20.3 s followed by 24°C DMF liquid for 6.1 s.

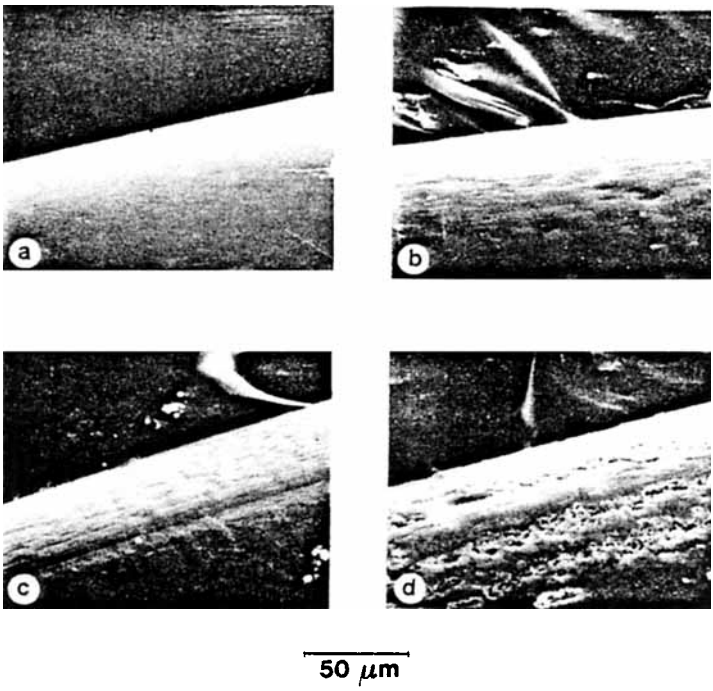

Fig. 21. Representative SEM's of the surfaces of undrawn PET filaments exposed to 50°C DMF vapor followed by 50°C DMF liquid. Residence times: (a) vapor 9.2 s, liquid 2.0 s; (b) vapor 8.4 s, liquid 3.6 s; (c) vapor 6.4 s, liquid 7.6 s; (d) vapor 2.5 s, liquid 15.3 s. Note that, as progressively shorter vapor precontact times are used, a cavitated surface structure becomes apparent.

resulted in the original treatments at this temperature. Progressively shorter vapor phase contact times were employed in this series of experiments. As expected, when the vapor contact time is greatly diminished, a cavitated surface structure becomes apparent. In this case the surfaces layer produced by vapor SINC becomes unstable to subsequent liquid swelling.

SUMMARY AND CONCLUSIONS

An anomalous temperature dependence of surface modification has been observed with as-spun PET fibers. A sudden disappearance of surface cavitation with increasing temperature was noted in both continuous and immersion-type treatments, with and without subsequent drawing, for both $MeCl_2$ and DMF solvent baths. It is felt to be a generally encountered phenomenon in attempting to produce surface modifications of solvent crystallizable substrates by open-bath solvent contact.

A qualitative description of the mechanism responsible for surface cavitation has been discussed. This mechanism postulates that surface cavitation is a natural consequence of the transport of interactive permeants in amorphous PET, which can be described as Case II diffusion coupled with rapid crystallization from the swollen state. Estimates of the ratio of the threshold concentration for swelling to the saturation concentration in amorphous domains for interactive and noninteractive permeants support this idea. Surface layers are

shown to have the highest potential for swelling before crystallization; hence highly cavitated surface structures occur. There is no indication that anomalous temperature effects should be associated with surface modifications based on this understanding. The observed temperature effects are attributed to an intervening phenomenon.

Analysis of penetration depth data indicates that this intervening phenomenon is surface localized. Detailed surface microscopy suggests the formation of smooth surface layers over normally observed cavitation at higher temperatures. Through systematic variation of treatment conditions, certain plausible origins of such a smooth surface layer are eliminated. By examination of vapor only treatments and through controlled vapor–liquid treatments, it is shown that precontact with vapor is most likely responsible for the elimination of surface cavitation at higher temperatures. A surface layer is produced by vapor phase SINC which, under conditions of sufficient severity (long contact times, high vapor activity), is stable when subjected to subsequent liquid treatment. As implied by the mechanism and supported experimentally, surface cavitation can be produced or eliminated at will, regardless of the liquid bath temperature, by controlling the extent and severity of vapor precontact.

These studies have been carried out under a grant from the National Science Foundation (Grant No. DMR-7905980). The authors appreciate helpful discussions with Professor William B. Russel, Princeton University Department of Chemical Engineering, and Dr. L. Rebenfeld, Textile Research Institute.

APPENDIX

References

1. P. J. Makarewicz, Ph.D. Thesis, Dept. of Chem. Eng., Princeton University, Princeton, N.J., 1977.
2. P. J. Makarewicz and G. L. Wilkes, *J. Polym. Sci., Phys. Ed.*, **16**, 1529 (1978).
3. P. J. Makarewicz and G. L. Wilkes, *J. Polym. Sci., Phys. Ed.*, **16**, 1559 (1979).
4. P. J. Makarewicz and G. L. Wilkes, *J. Appl. Polym. Sci.*, **23**, 1619 (1979).
5. H. Jameel, J. Waldman, and L. Rebenfeld, *J. Appl. Polym. Sci.*, **26**, 1795 (1981).
6. E. A. Gerold, L. Rebenfeld, M. G. Scott, and H.-D. Weigmann, *Text. Res. J.*, **49**, 652 (1979).
7. H. L. Frisch, *Polym. Eng. Sci.*, **20**, 2 (1980).
8. B. R. Baird, H. B. Hopfenberg, and V. T. Stannett, *Polym. Eng. Sci.*, **11**, 274 (1971).
9. H. B. Hopfenberg, R. H. Holley, and V. T. Stannett, *Polym. Eng. Sci.*, **20**, 2 (1980).9, 242 (1979).
10. G. Astarita and G. C. Sarti, *Polym. Eng. & Sci.*, **18**, 388 (1978).
11. G. Astarita and S. Joshi, *J. Membr. Sci.*, **4**, 165 (1978).
12. B. H. Knox, H.-D. Weigmann, and M. G. Scott, *Text. Res. J.*, **45**, 203 (1975).
13. A. Peterlin, *Makromol. Chem.*, **124**, 136 (1969).
14. G. C. Sarti, *Polymer*, **20**, 827 (1979).
15. N. Thomas and A. H. Windle, *J. Membr. Sci.*, **3**, 337 (1978).
16. F. N. Kelley and F. J. Bueche, *J. Polym. Sci.*, **50**, 549 (1961).
17. R. S. Ware, S. Tirtowidjojo, and C. Cohen, *J. Appl. Polym. Sci.*, **25**, 2975 (1981).
18. W. R. Moore and R. P. Sheldon, *Polymer*, **2**, 315 (1961).
19. J. S. Vrentas and J. L. Duda, *Macromolecules*, **9**, 785 (1976).
20. J. S. Vrentas and J. L. Duda, *J. Polym. Sci., Phys. Ed.*, **15**, 417 (1977).
21. B. Meissner, *J. Polym. Sci., Polym. Lett. Ed.*, **19**, 137 (1981).
22. A. Peterlin, *J. Macromol. Sci., Phys. Ed.*, **11**, 57 (1975).

23. K. Bredereck, H. Dolmetsch, E. Koch, and R. Schoner, *Milliand Textilber.*, **56**, 50 (1975).
24. E. Schuller and M. Jansch, *Faserforsch. Textiltech.*, **14**, 97 (1963).
25. Brit. Pat. 1-546-914 (May 31, 1979).

Received February 16, 1982
Accepted April 26, 1982